Vol. **111** (2007) *ACTA PHYSICA POLONICA A* No. 4

Proceedings of the XII National School "Correlated Electron Systems...", Ustroń 2006

Manifestation of Electron Correlations in the V_2O_3 and NiS_2 Systems

J.M. Honig

Department of Chemistry, Purdue University
West Lafayette, IN 47907-2084, USA

Dedicated to Professor Józef Spałek on the occasion of his 60th birthday

The experimental manifestation of electron correlation effects in the V_2O_3 and NiS_2 systems are reviewed, and recent elementary theories for interpreting the many different types of metal–insulator transitions based on these theories are provided. Research on the critical phenomena displayed by the interacting electrons in these systems is also reviewed.

PACS numbers: 71.30.+h, 71.28.+d, 72.80.Ga

1. Introductory comments

Among his many scientific achievements Józef Spałek has contributed greatly to our understanding of the experimental manifestations of electron correlation effects in solids. This has been very useful in the proper characterization of a several different metal–insulator transitions that were very puzzling at the time they were being investigated in our laboratory. It therefore seemed appropriate to selectively highlight in this article some of the key experiments, as well as their theoretical interpretation by Spałek and collaborators.

One of the hallmarks of Spałek's work is the basic simplicity of the fundamental concepts, although the mathematical elaboration of the fine details inevitably becomes rather cumbersome. In the present, rather personalized, article we emphasize the elementary steps needed for a rationalization of selected data. The reader is urged to consult the references cited below as well as several review articles [1] for a much more balanced and complete exposition of the subject matter.

2. Experimental data

We begin with a brief review of experimental resistivity measurements on systems that manifest a variety of metal–insulator transitions: V_2O_3, Cr- and Ti-doped V_2O_3, nonstoichiometric V_2O_3, and the NiS_2-NiSe_2 system. Work on the vanadium sesquioxide system was initiated by Foëx [2] who was the first to report a discontinuous change in electrical properties in V_2O_3. A highly cited set

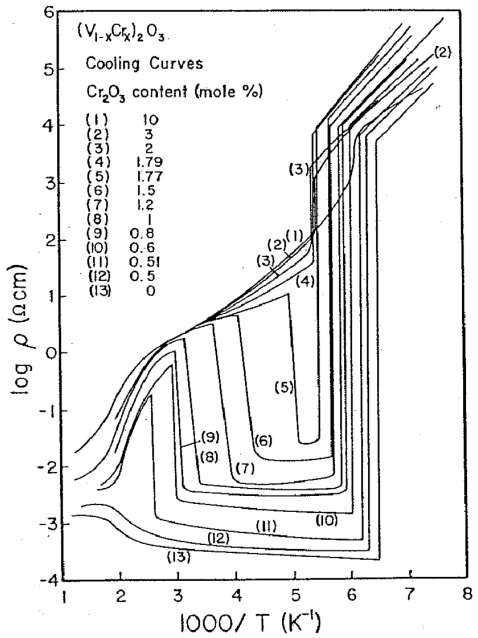

Fig. 1. Electrical resistivity measurements on $(V_{1-x}Cr_x)_2O_3$ single crystals plotted logarithmically against reciprocal temperature. Let us note the various types of transitions discussed in the text.

of papers by the Bell group [3] drew attention to many different manifestations of electron correlation effects in the $(V_{1-x}Cr_x)_2O_3$ system. Figure 1 displays a much more extensive set of electrical resistivity data by the Purdue group [4] for $(V_{1-x}Cr_x)_2O_3$ with $0 \leq x \leq 0.1$. Particularly striking are the many different types of observed electrical transitions. Broadly speaking, all members in this group are antiferromagnetic insulators (AFI) at low temperatures. With rising temperature T, materials in the composition range $0 \leq x \leq 0.005$ experience a transformation to a paramagnetic metallic (PM) phase. This transition can be suppressed by doping V_2O_3 with small amounts of Ti, or by rendering the material slightly non-stoichiometric [5], so that these compositions remain relatively good conductors at all temperatures. In the composition region $0.0177 \leq x \leq 0.051$ while increasing the temperature beyond the stability range of the AFI regime, one encounters a transition first from the PM state to a paramagnetic insulator (PI), and then back to a second metallic phase (PM′). This regime of reentrant metallic behavior, which had escaped earlier notice, is rare in oxides and is therefore of special interest. Lastly, for $x > 0.018$ only the AFI–PI transformation is encountered. These observations immediately raise the question whether a single mechanism can be devised for explaining all the different types of transformations and further, how thermal inputs of order $k_BT \approx 10$ meV can generate changes in electronic structure that typically amount to 2 eV. These matters are addressed below.The electrical

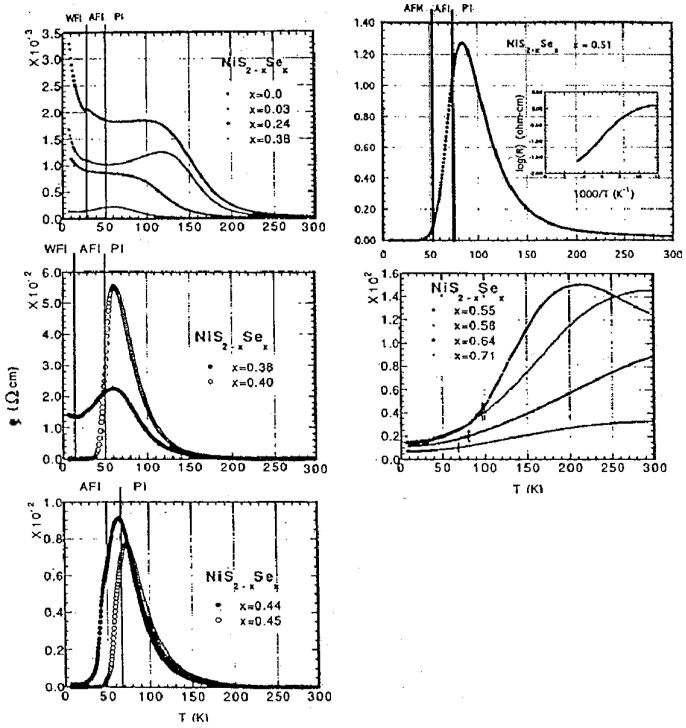

Fig. 2. Electrical resistivity measurements on $NiS_{2-x}Se_x$ single crystals plotted logarithmically against temperature. Let us note the changes in properties, discussed in the text, as S is replaced by Se.

properties of the $NiS_{2-x}Se_x$ system raise related questions. Work in this area was initiated by the duPont group [6] and extended at Purdue University and at the University of Kentucky [7]. Resistivity measurements are displayed in Fig. 2 in the range $0 \leq x \leq 0.71$. One should note the plateau in the region 30–120 K at compositions $0 \leq x \leq 0.24$ that separates the low temperature AFI phase (the magnetic moments are actually canted, rendering these compounds slightly ferromagnetic) from the PI phase. This has recently been traced [8] to the existence of a metallic surface layer and is not associated with bulk properties. However, in the range $0.38 \leq x \leq 0.52$, the compounds are metallic at low T, followed by an opening of a gap in the density of states near 50–70 K as manifested by a metal–insulator transition that renders the material semiconducting at higher T. This is the reverse of normal metal–insulator transitions and is therefore counterintuitive. Lastly, for increasing $x > 0.55$ the transition to the PI state gradually fades; the material then remains a conductor at all T. One should also be aware that in this system the so-called metallic phase has a resistivity as high as 140 Ω cm, which is a full ten orders of magnitude larger than that of highly pure Cu metal at comparable temperatures. These various observations again require explanation.

The interpretation of these phenomena is based on a model, originally advanced by Gutzwiller [9] and by Brinkman and Rice [10], in which the insulating state of these systems arises from a balance between itinerant Bloch-type band states and electron localization effects induced by mutual Coulomb repulsions between interacting electrons. A reformulation by Spałek and co-workers [11] permitted an extension of these concepts to nonzero temperatures. This renders plausible the view that in poor conductors a metal–insulator transition is linked to a changeover from band itineracy to a localized regime; the manner in which this is realized is the principal subject of the present article.

The question first arises as to why the V_2O_3 and NiS_2 systems are representative candidates for exhibiting electron correlation effects. In V_2O_3 the cation, element 23 in the fourth row of the periodic table, is just at the edge of significant overlap between cationic and anionic orbitals: Ti_2O_3 immediately to the left is a reasonably good conductor, whereas Cr_2O_3 immediately to the right is an excellent insulator. Accordingly, doping of V_2O_3 with Ti or Cr renders the parent compound more conducting or more insulating, thereby permitting an adjustment of the relative importance of itinerant vs. localized properties. NiS_2 is a semiconductor; by admixture of Se, which lies immediately below S in the periodic table, with a correspondingly larger radial extension of its orbitals, one improves the cation–anion orbital overlap to the point where a changeover to a conducting state becomes possible.

We next turn to a more quantitative assessment of these ideas.

3. Thermodynamic considerations

Hereafter we will no longer consider the low-T transitions in Fig. 1 that pertain to the AFI phase, for these transformations involve both a change in crystal structure and magnetic ordering phenomena that are beyond the purview of the present paper. We thus begin our study of the remaining metal–insulator transitions with a very simplistic but effective thermodynamic argument. Let us consider a localized electron system with one potentially mobile electron per atom in a regular lattice of N sites, whose zero of energy E is the energy of each electron at its regular lattice site at $T = 0$. The electron may be placed into position in either a "spin up" or a "spin down" configuration. The corresponding entropy for each electron is thus $S_l/N = k_B \ln 2$ and the Helmholtz energy per electron is then

$$F_l/N = E_l/N - TS_l/N = -k_B T \ln 2. \tag{1}$$

This function changes linearly with temperature. This situation should be contrasted with the itinerant electron picture. We start with the Sommerfeld model of an electron gas whose low-T heat capacity per electron per site is given by $C_i/N = \gamma T$; we show later how the linear coefficient γ for an interacting electron gas is related to γ_0 for a noninteracting gas. The energy of the itinerant electron gas is then given by $E_i/N = \int (C_i/N) \mathrm{d}T = E_0/N + \frac{1}{2}\gamma T^2$, where E_0 is a constant to be specified later. The corresponding entropy is $S_i/N = \int \gamma \mathrm{d}T = \gamma T$, whence the Helmholtz free energy for the itinerant state is

$$F_i/N = E_i/N - TS_i/N = E_0/N - \tfrac{1}{2}\gamma T^2. \tag{2}$$

This quantity varies parabolically with temperature. In Fig. 3 we compare the two free energies: the localized case is represented by the straight line that passes through the origin of coordinates, whereas the various parabolas intersect the ordinate at values E_0. If E_0 has a large negative value (curve 1), the parabola always lies well below the straight line; thus, the itinerant state always has the lower free energy and therefore is the stable phase. However, for energies in a fairly wide range of negative E_0 values, curves 3a and 3b, the parabola intersects the straight line at two places: the itinerant regime still has the lower free energy for temperatures below L or J. But in the intermediate range LM or JK the localized configuration has the lower free energy. Finally, for temperatures beyond M or K the metallic state once again has the lower free energy. This represents the case of reentrant metallic behavior, seen in the $(V_{1-x}Cr_x)_2O_3$ system as described above.

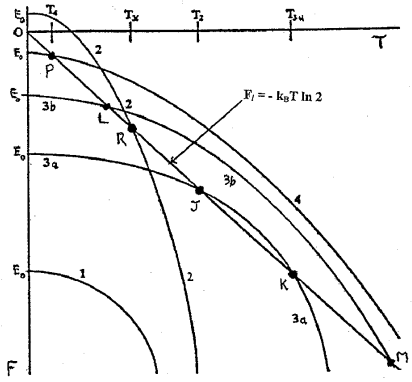

Fig. 3. Sketch of the free energy as a function of temperature for localized electrons (straight line) and for itinerant electrons (parabolas, intersecting the ordinate at various values of E_0). The intersection points at various temperatures indicate conditions where phase transitions occur. Let us note in particular the double intersections between the straight line and some of the parabolae.

Actually, the high temperature PI–PM′ transformation is not sharp, as anticipated, but stretches out over a significant interval, presumably because at higher T the lattice can adjust to a change in electron configuration — a feature that has been left out of account. Let us note that since the slopes of the straight lines and the parabolas change discontinuously at the intersection points the entropy of the PM and PI phases differ, so that the transitions are of first order. Further, there exists a value of E_0 (not shown) where the parabolas and straight lines are tangent to each other at a temperature T_c; thus, at that critical point one deals with a higher order phase transformation.

As E_0 becomes yet less negative, the parabola (curve 4) intersects the straight line at a low temperature P: this is a somewhat unusual case in which the low

temperature phase is metallic and the high temperature phase is insulating. Such a situation was encountered in the $NiS_{2-x}Se_x$ system in the composition range $0.35 < x < 0.58$. Actually, a second intersection point must be present, but it occurs at a high temperature where the material is no longer stable. Lastly, for small positive values of E_0 the parabola (curve 2) intersects the straight line at a temperature R. This represents the more usual case for which the insulating state is stable at low T and a first-order transition to the metallic state then takes place at higher temperatures.

This very rudimentary description catches the essence of a metal–insulator transformation driven by electron correlation effects; we provide a better rationale below. We next determine the value of E_0. At this very elementary level we argue as follows. An electron gas distributed in a partially filled energy band has an average kinetic energy $E_i/N = -|\bar{\varepsilon}|$. To take electron correlations into account we adopt the Hubbard model. We posit that electron interactions may be ignored except when two electrons reside on the same atom with reversed spins, in which case their interaction energy is represented by the Hubbard parameter U. Let the probability of a double site occupancy be η; then the average Coulomb repulsion energy per electron is given by $U\eta > 0$. One must also mimic the hindered motion of the interacting electrons as they move past each other. This is attended to by introducing a correction factor $0 < \Phi(\eta) < 1$, whose precise form is specified later. We thus write

$$E_0/N = -\Phi(\eta)|\bar{\varepsilon}| + U\eta. \tag{3}$$

This formulation is highly suggestive. It shows that there can exist conditions under which the negative electronic kinetic energy is almost compensated for by the positive repulsion energy, thereby rendering E_0/N very small. Then the free energy is determined largely by the entropic contributions, yet to be determined, that are very sensitive to temperature changes. It is in this regime of near balance that electronically driven metal–insulator transformations are encountered. This discussion thus rationalizes at an elementary level how thermal input energies can initiate large electronic energy shifts.

4. Determination of scaling function

For a more sophisticated introduction to electron correlation effects for a half-filled energy band we follow the lead of Spałek et al. [11, 12] who replaced the set of interacting electrons by a collection of independent quasiparticles with momenta $\hbar k$ ($\hbar$ being the Dirac constant and k — the wave vector) and energies E_k. The cardinal step here is the positing of the relation $E_k = \Phi(\eta)\varepsilon_k$ as a scaling function that relates the energies of the quasiparticles to those of the bare electrons, ε_k. This approach is justified a posteriori by its success. The individual band energy of each of the N quasiparticles is then given by

$$E_{\mathrm{B}}/N = \int_{-\infty}^{\infty} Ef(E)\rho(E)\mathrm{d}E, \tag{4}$$

where $f(E) \equiv f[(E - E_{\rm F})/k_{\rm B}T]$ is the Fermi–Dirac energy distribution which, by definition, holds for the independent particle assembly; here $E_{\rm F}$ is the Fermi energy and $\rho(E)$ is the appropriate density-of-states (DOS) function. We now introduce the scaling law into the above to obtain

$$f(E) \equiv f[(E - E_{\rm F})/k_{\rm B}T] = f[(\varepsilon_k - \mu)/k_{\rm B}T^*] \equiv f^*(\varepsilon_k), \tag{5}$$

in which $\mu \equiv E_{\rm F}/\Phi$ is the Fermi energy of the bare particles and $T^* \equiv T/\Phi$ is an effective temperature that governs the energy distribution of the bare electrons associated with the quasiparticles.

Based on the mathematical relation governing the Dirac delta distribution, $\delta(ax) = |a|^{-1}\delta(x)$, the DOS function for electrons of spin σ may now be rewritten as a sum of Dirac delta distributions as follows:

$$N\rho^\sigma(E) = \sum_k \delta[\Phi(\varepsilon - \varepsilon_k)] = \Phi^{-1}\sum_k \delta(\varepsilon - \varepsilon_k) = \Phi^{-1}(\eta)\rho_0^\sigma(\varepsilon)N. \tag{6}$$

Thus, the DOS for the correlated electrons, ρ^σ, is increased by the yet-to-be established factor $\Phi^{-1} > 1$ relative to the DOS of the bare electrons, ρ_0^σ. As a result, the band width is narrowed and the effective mass of the charge carriers is increased relative to those of the bare electrons. Now introduce (6) and (5) in (4) to obtain

$$E_{\rm B}/N = \Phi(\eta)\int_{-\infty}^{\infty} \varepsilon f^*(\varepsilon)\rho_0^\sigma(\varepsilon){\rm d}\varepsilon \equiv \Phi(\eta)\overline{\varepsilon}(T^*), \tag{7}$$

where $\overline{\varepsilon}$ is the average kinetic energy per bare electron at an effective temperature T^*. We thereby recover the first term in Eq. (3). Since the scaling function $\Phi(\eta)$ depends on the average double occupancy of any site, η, we can simply adjoin to Eq. (7) the local electron site interaction energy U for double occupation, multiplied by the probability η of its occurrence. When added to Eq. (7) one recovers Eq. (3).

5. Specification of scaling function Φ at $T = 0$

In what follows we adopt for simplicity the rectangular density-of-states function (RDOS) in the form $\rho_0^\sigma = 1/W$ for $-W/2 \le \varepsilon \le W/2$ and $\rho_0^\sigma = 0$ outside this range; W is the bandwidth of the bare band; this form of the RDOS applies to occupation by an electron with a given spin. We let n represent the particle number operator for occupation of a representative site by an electron.

To determine Φ we note that the maximum value for double occupancy is $\eta = \frac{1}{4}$ for a half-filled nondegenerate band. It is therefore apposite to introduce a Taylor series expansion in the form $\Phi(\eta) = f_0 + f_1\eta + f_2\eta^2 + \ldots$ The coefficients f_i and the optimal value of η may be found by imposing constraints: (i) Minimize $E_{\rm G}/N$ with respect to η to determine the optimal value η_0. (ii) Set $U = 0$; the sites are then occupied randomly, whence the average kinetic energy is given by $\overline{\varepsilon} = -W(n/2)(1 - n/2)$, where the last factor involves the probability that a bare electron with a given spin can move to an adjacent site that is not already occupied by another bare electron of the same spin. Moreover, for $U = 0$, (iii) $\Phi = 1$ and $\eta_0 = n^2/4$. (iv) When $\eta = 0$, double site occupancy is prohibited;

the average bare electron kinetic energy is now $\bar{\varepsilon} = -W(n/2)(1-n)$, where the second factor involves the probability that an adjacent empty site is available for occupancy. Elementary algebraic manipulations then lead to the results $f_0 = (1-n)/(1-n/2)$, $f_1 = 4/[n(1-n/2)]$, $f_2 = -8/[n^3(1-n/2)]$. These quantities may then be substituted in Eq. (3) to find the dependence of double occupancy, the correlation function, and the band energy in their dependence on U and W for various n.

Considerable simplification is achieved by treating the case of a half-filled band, $n = 1$, which, in the RDOS approximation leads to the results

$$\eta_0 = (1/4)(1 - U/2W), \tag{8a}$$

$$\Phi(\eta_0) = 8\eta_0(1 - 2\eta_0) = 1 - (U/2W)^2, \tag{8b}$$

$$E_0/N = -(W/4)(1 - U/2W)^2. \tag{8c}$$

We see that due to correlations the average band energy $-W/4$ for bare electrons is now reduced by the factor $(1 - U/2W)^2$; the band narrowing factor $\Phi(\eta_0) \leq 1$ is specified by (8b). Clearly, for $U > 2W$ the above quantities assume unphysical values; thus, a Mott–Hubbard type of localization must set in at the critical value $U = 2W$ for a rectangular density of states.

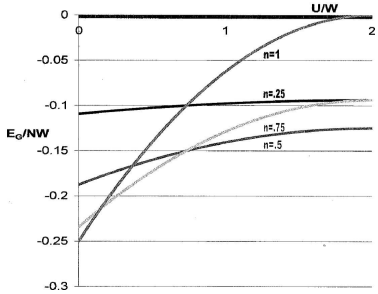

Fig. 4. Plots of reduced band energies $E_{\rm G}/NW$ vs. U/W for a RDOS at different values of n. The left and right end points represent respectively reduced energies prevailing in the absence of electron interaction and in strong interactions such that $U/2W = 1$. Let us note the reduction in energy spread as n diminishes. R. Hoehn, unpublished work.

To gain a better feel for the effects of deviating from the half-filled band scenario we exhibit in Fig. 4 a new plot showing how the reduced band energies at 0 K change with U/W for various n values. The calculations are based on the generalized, much more complicated form of Eqs. (8) when $n \neq 1$. The results clearly indicate the diminishing spread of the energy scale as n diminishes, as well as the concomitant variations of $E_{\rm G}/NW$ with U/W as n is altered.

6. Extension to nonzero temperatures

The case of nonzero temperatures for interacting electrons was first considered by Spałek and co-workers [11, 12]. When $T > 0$ the entropy contribution

must be added to the energy of the quasielectron assembly. We now differentiate between the two distinct spin alignments $\sigma = \pm 1/2$. This free energy per site is then specified by

$$F_i/N = (1/N)\sum_{k\sigma} E_{k\sigma} f(E_{k\sigma}) + U\eta + (k_{\mathrm{B}}T/N)\sum_{k\sigma}\{f(E_{k\sigma})\ln f(E_{k\sigma}) + [1 - f(E_{k\sigma})]\ln(1 - f(E_{k\sigma}))\}. \tag{9}$$

On now substituting Eq. (5) and $T = T^*\Phi$ in Eq. (9) one obtains the simple scaled relation

$$F_i(T)/N = \Phi(\eta)F_0(T^*)/N + U\eta, \tag{10}$$

where $F_0(T^*)$ is the free energy of the bare electron assembly at the effective temperature T^*, namely

$$F_0(T^*) = \sum_{k\sigma} \varepsilon_{k\sigma} f^*(\varepsilon_{k\sigma}) + k_B T^* \sum_{k\sigma}\{f^*(\varepsilon_{k\sigma})\ln f^*(\varepsilon_{k\sigma}) + [1 - f^*(\varepsilon_{k\sigma})]\ln(1 - f^*(\varepsilon_{k\sigma}))\}. \tag{11}$$

This shows the one-to-one correspondence between the bare and interacting electrons at all temperatures, thereby also providing an a posteriori justification for introducing the concept of quasiparticles. Moreover, we can immediately apply the Sommerfeld model to determine the low-temperature heat capacity per site of the independent quasiparticles in the form

$$C_i/N = \gamma(E_{\mathrm{F}})T, \quad \gamma \equiv 2\pi^2 k_{\mathrm{B}}^2 \rho^{\sigma}(E_{\mathrm{F}})/3 = 2\pi^2 k_{\mathrm{B}}^2 \rho_0^{\sigma}(\varepsilon_{\mathrm{F}})/3\Phi \equiv \gamma_0/\Phi, \tag{12}$$

where we used (6) to replace the DOS per spin for the quasiparticles, ρ^{σ}, with that for the bare particles, ρ_0^{σ}. For a RDOS $\rho_0^{\sigma} = 1/W$. We can then determine the low-temperature energy of the quasiparticle assembly via $\int (C_i/N)\mathrm{d}T = E_0/N + \frac{1}{2}\gamma T^2$, where E_0 is specified by Eq. (7). Introducing Eq. (12) we find

$$E_i(T)/N = -\Phi|\bar{\varepsilon}| + U\eta + \gamma_0 T^2/2\Phi. \tag{13}$$

The entropy is specified by $\int (C_i/TN)\mathrm{d}T$, so that

$$S_i(T)/N = \gamma_0 T/\Phi. \tag{14}$$

Finally, the Helmholtz free energy functional is given by

$$F_i/N = -\Phi(\eta)|\bar{\varepsilon}| + U\eta - \gamma_0 T^2/2\Phi, \tag{15a}$$

which is not the same as the Helmholtz free energy since the extrathermodynamic variable η has not yet been optimized. This, in fact, is the next step: as shown by Spałek et al. [11], on imposing the constraint $(\partial F_i/\partial\eta) = 0$ and for $n = 1$ one obtains the low-T limiting expressions for η_0 and for Φ_0 identical with Eqs. (8a) and (8b). The optimized Helmholtz free energy expression thus has the RDOS form ($n = 1$)

$$\frac{F_{i0}}{NW} = -\frac{1}{4}\left[1 - \left(\frac{U}{2W}\right)^2\right] + \frac{U}{4W}\left(1 - \frac{U}{2W}\right) - \frac{1}{2}\frac{\gamma_0 T^2}{W[1 - (u/2W)^2]}, \tag{15b}$$

that involves solely the parameter ratios U/W and γ_0/W, as well as the T^2 dependence. The above is of the form specified by Eq. (2) and thus furnishes the rationale for the associated qualitative discussion. The above expressions have been generalized by Spałek and co-workers [11, 12] who developed a two-fluid model for the interacting electron assembly. They further took into account the very interesting effects developed in an external magnetic field and considered the expansion of the various thermodynamic quantities in higher powers of the temperature.

For the localized phase we write, as before,

$$F_l/NW = -(k_{\mathrm{B}}T/W)\ln 2. \tag{16}$$

We can now determine the intersection points sketched in Fig. 3. Transitions between the itinerant and localized states occur whenever the corresponding free energies match. On equating Eqs. (15b) and (16) one obtains a quadratic equation in $k_{\mathrm{B}}T/W$ with the two roots

$$\left(\frac{k_{\mathrm{B}}T}{W}\right)_{\pm} = \frac{3}{2\pi^2}\left[1-\left(\frac{U}{2W}\right)^2\right]\left\{(\ln 2) \pm \left[(\ln 2)^2 - \frac{\pi^2}{3}\left(\frac{1-U/2W}{1+U/2W}\right)\right]^{1/2}\right\}. \tag{17}$$

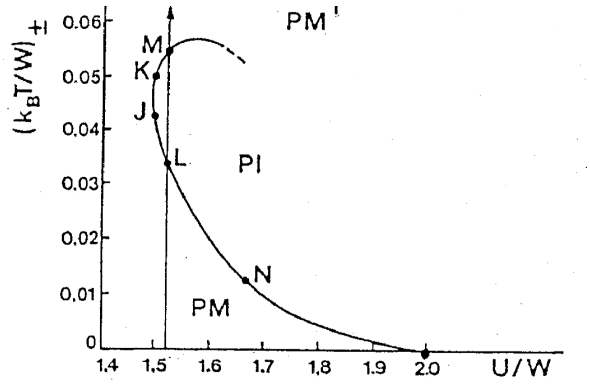

Fig. 5. Coexistence curve for delineating the phase boundaries of the PM, PI, PM′ regions in the phase diagram of the reduced temperature vs the reduced Hubbard parameter. The retrograde curve was truncated as indicated in the text.

A plot of $k_{\mathrm{B}}T/W$ vs. U/W is shown in Fig. 5. The retrograde curve represents the phase boundary separating the insulating, localized regime (PI) from the itinerant, metallic regimes, PM and PM′. In examining the results one should remember the inherent restrictions: the curve is obtained in the low-temperature limit for a half-filled, nondegenerate band, using an RDOS for which $\rho_0^{\sigma} = 1/W$. The phase boundary has been artificially terminated both at $T = 0$ and at a point where the low-T approximation breaks down. Several matters are of interest: (i) There exists

a critical limit $(U/W)_l$ at the coalescence point $(k_BT/W)_+ = (k_BT/W)_- \approx 0.045$, corresponding to $U/W \approx 1.49$; below this reduced correlation energy the metallic configuration is stable at all temperatures. This conforms to the qualitative understanding that on-site interaction energies must exceed a temperature-dependent critical value for electron correlation effects to force a phase transition. (ii) At $T = 0$ the itinerant metallic state is stable up to the critical value $(U/W)_0 = 2$. Beyond that point the electrons are completely localized, so long as $n = 1$. (iii) Another critical point is reached close to the cutoff at $k_BT/W \approx 0.045$, $U/W \approx 1.55$. At higher reduced temperatures and for any value of U/W the PM′ and PI phases become indistinguishable in a manner reminiscent of the conventional liquid water–water vapor critical point. (iv) On raising the reduced temperature of a material with fixed U/W in the limited range $1.49 < U/W < 1.56$ one encounters the sequential phase change PM–PI–PM′ characteristic of reentrant metallic behavior. This approach therefore captures the essentials of the transitions encountered in the $(V_{1-x}Cr_x)_2O_3$ system over the limited range $0.005 < x < 0.018$. (v) In the range $1.56 < U/W < 2$ only the PM–PI transformation is encountered with rising reduced temperature, as is experimentally found to be the case for $x > 0.018$. Finally, for U/W close to the critical value of 2 the metallic phase is stable only over a very low set of reduced temperatures and results in the PM–PI transition with rising temperature; this case is exemplified by the $NiS_{2-x}Se_x$ system for $0.35 < x < 0.55$.

This very simplistic presentation does mimic the transitions observed in the magnetically disordered phases of the V_2O_3–Cr_2O_3 and NiS_2−$NiSe_2$ systems, evaluates the range of permissible parameters, and thereby provides a reasonably quantitative interpretation for the experimental observations.

7. Heat capacity measurements

Aside from the above considerations one would like more direct experimental confirmation of the presence of electron correlation effects. Several of these are reviewed in a recent publication [13]. Here we concentrate on heat capacity measurements: as shown in Eq. (12), relative to the Sommerfeld value for bare electrons at low temperatures, the heat capacity is increased by the factor $1/\Phi = [1 - (U/2W)^2]^{-1}$ in the RDOS approximation. In Fig. 6, bottom curve, there is shown a set of experimental heat capacity measurements [14] on nonstoichiometric V_2O_3 under pressures sufficient to render the material barely metallic. Let us note that the indicated γ values exceed by a factor of twenty to fifty the electronic contributions to the heat capacities of normal metals. Further, as the pressure is relaxed the lattice expands, the conduction band narrows, and the electron correlations increase. Correspondingly, one observes a rise in γ as the system approaches the metal–insulator boundary. Vacancies in the cation sublattice of $V_{2-y}O_3$ mask the anticipated indefinite rise of γ as the metal–insulator boundary is reached. This is verified by the top curve in Fig. 5, where γ is shown to depend on the extent of departure from ideal stoichiometry.

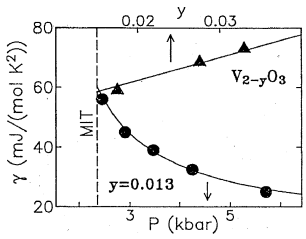

Fig. 6. Electronic contribution γ to the low-temperature heat capacity of $V_{2-y}O_3$ under pressure (lower curve, $y = 0.013$) and as a function of y (upper curve). Let us note the increase in γ as the metal–insulator boundary is approached by release of pressure on the crystal.

Complementary investigations were earlier carried out on metallic $(V_{1-x}Ti_x)_2O_3$ by the Bell group [3] with very similar results. They reported γ values of 40–80 mJ/(mol K^2) for barely metallic $(V_{1-x}Ti_x)_2O_3$ for x value in the range 0.05 to 0.08. Comparable studies on $NiS_{2-x}Se_x$ [15] led to γ values in the range of 40–50 mJ/(mol K^2) for barely metallic samples with $0.51 < x < 0.58$. All of the above results indicate that the Sommerfeld heat capacity constants for correlated metals fall in the same range of values which is much larger than for ordinary metals, as expected for materials displaying significant electron correlation effects.

8. Critical phenomena of correlated electron systems

The systems considered above lend themselves to a study of electronic behavior at a critical point. As mentioned earlier, one anticipates conditions where the

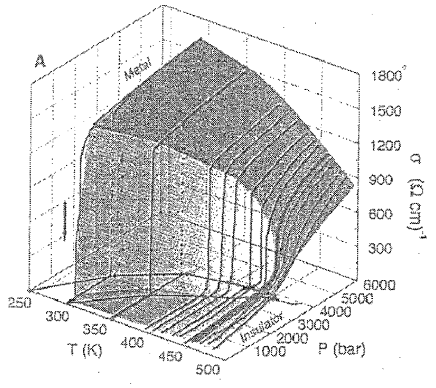

Fig. 7. The electrical conductivity σ of a $(V_{0.989}Cr_{0.011})_2O_3$ single crystal as a function of decreasing or increasing pressure at temperatures close to the critical temperature. Let us note the discontinuity in σ at the transition for $T < T_c$ which gives way to a continuous change in σ for $T > T_c$.

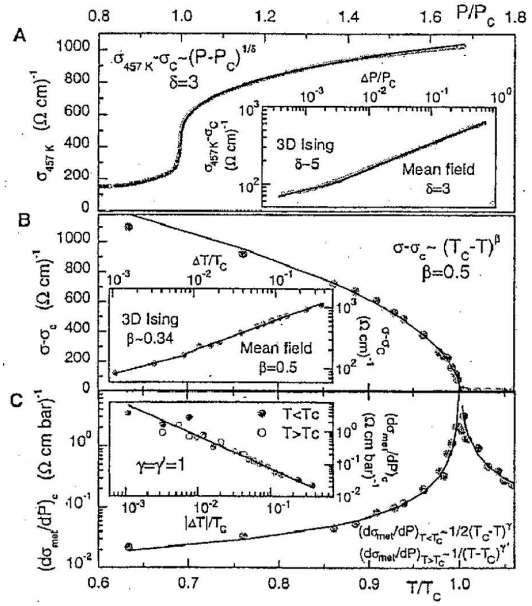

Fig. 8. (A) Electrical conductivity measurements as a function of reduced pressure at the critical temperature of 457 K. Inset shows the double logarithmic plot that provides the critical exponents $\delta = 3$ or 5 under conditions relatively far removed from or close to the critical value of P_c. (B) Plot of $\sigma - \sigma_c$ as a function of $(T_c - T)$. Inset shows a double logarithmic plot that yields a critical exponent $\beta = 0.5$ or 0.34 under conditions relatively far removed from or close to the critical value of T_c. (C) Pressure derivative of the electrical conductivity σ as a function of the reduced temperature close to the critical point. Inset shows double logarithmic plot that yields a critical exponent $\gamma = \gamma' = 1$ both above and below the critical temperature.

distinction between the PM and PI phases in the $(V_{1-x}Cr_x)_2O_3$ system ceases to exist. The appropriate temperature and composition where this occurs were first experimentally identified by Kuwamoto and co-workers [4]. A detailed investigation of the critical phenomena, shown in Fig. 7, was undertaken by Limelette et al. [16] who reported the electrical conductivity σ of $(V_{1-x}Cr_x)_2O_3$ with $x = 0.011$ as a function of temperature T and pressure P close to the critical point. At moderately high pressures of several kbar the material is metallic; on release of pressure the insulating state is reached. The transition occurs discontinuously below the critical temperature of $T_c = 457$ K and continuously above T_c. The critical point is marked by a continuous curve with an infinite slope. Details of these investigations are exhibited in Fig. 8. The top part shows the variation of σ with pressure at 457 K. The double logarithmic inset indicates that $\sigma - \sigma_c \sim (P - P_c)^{1/\delta}$ with $\delta = 3$ relatively far from the critical point, and $\delta = 5$ very close to the critical point. These numbers agree respectively with $\delta = 3$ for the mean field theoretical

description of the critical exponents of fluids, and with the exponent $\delta = 4.814$ derived on the basis of renormalization group techniques.

The central part shows the temperature dependence of the conductivity under pressure: the double logarithmic plot indicates that $\sigma - \sigma_c \sim (T - T_c)^\beta$ with $\beta = 0.5$ in a range relatively far removed from criticality. This accords with the mean field value anticipated for fluids. Closer to the critical point they obtained $\beta = 0.34$, as compared to the theoretical value of $\beta = 0.327$ derived by group renormalization techniques.

The third part shows the pressure derivatives of the electrical conductivity as a function of T/T_c both above and below the critical temperature. These workers found that $(\partial\sigma/\partial P) \sim (1/2)(T - T_c)^\gamma$ for $T < T_c$ and $(\partial\sigma/\partial P) \sim 1/(T - T_c)^{\gamma'}$ for $T > T_c$ with $\gamma = \gamma' = 1$. These are analogues of the isothermal compressibility, with the same values as in the mean field approximation. Any deviations closer to the critical points could not be established due to the scatter of the data.

The above information clearly shows that this interacting electron assembly generates critical point phenomena completely analogous to those of ordinary fluids. Limelette and co-workers interpret this to mean that near criticality the insulating phase is constituted by V^{3+} ions with a wide separation between coexisting V^{4+} and V^{2+} ions, to form the analogue of the gaseous state. By contrast, the metallic state, with a sizeable density of V^{4+} (hole configuration) and V^{2+} (electron configuration) is comparable to a liquid.

The $NiS_{2-x}Se_x$ system with $x = 0.44$ has been used by the Chicago group [17] to investigate quantum critical phenomena close to absolute zero. Such transitions are driven not by thermal effects but by quantum mechanical fluctuations. The energy scales entering the problem now also involve time scales that are set by Planck's constant and the characteristic energy of the system. The choice of the above compound is dictated by its proximity close to the metal–insulator boundary: it is barely metallic under moderate pressures but becomes an insulator under ambient conditions.

To interpret the results we resort to a conventional analysis [18] of quantum critical effects. Let K be a control variable of interest and let $\delta \equiv K - K_c$, where K_c is its value at the critical point. Typical of all critical phenomena, it is assumed that when $\delta > 0$ the correlation length ξ, over which the various physical characteristics of the system vary reasonably uniformly, diverges as $\xi(K) \sim |\delta|^{-\nu}$. There exists a corresponding divergence in the time scale: it takes longer times to establish physical uniformity over greater distances. One thus sets up a divergent time scale $\xi_\tau(K) \sim \xi^z$. At $T = 0$ and near criticality any quantum mechanical operator O that depends on wave number k, angular frequency ω, and on K is assumed to follow the diverging relation

$$O(k, \omega, K) = \xi^d O(k\xi, \omega\xi_\tau) = |\delta|^{-d\nu} O(k\xi, \omega\xi_\tau), \tag{18}$$

where the operator on the right is independent of K and thus, of no immediate interest.

The situation for $T > 0$ is more complicated. It is based on the classical partition function $Z(\beta) = \mathrm{tr}\exp(\beta_t \hat{H})$, where tr is the trace over all accessible states of the system, $\beta_t \equiv 1/k_\mathrm{B}T$ and $\hat{H}$ is the quantum mechanical operator of interest. That formulation is to be compared with the quantum mechanical expression $\exp(\mathrm{i}\hat{H}\tau/\hbar)$ for the time evolution of the operator $\hat{H}$. This invites the comparison relation $\tau = -\mathrm{i}\hbar$ that is commonly cited. For $T = 0$ the time scales are infinite, but for $T > 0$ one encounters an upper limit $L_\tau = -\mathrm{i}\hbar/k_\mathrm{B}T$ on τ. Thus, for $T > 0$ Eq. (18) must then be modified to read

$$O(k, \omega, K, T) = L_\tau^{d/z} O(kL_\tau^{d/z}, \omega L_\tau, L_\tau/\xi_\tau), \tag{19}$$

where the factor on the right does not contain K and again is not of immediate interest.

The above two relations form the basis for interpreting the experiments. Figure 9 shows the electrical conductivity σ at 50 mK as a function of pressure P close to the critical pressure P_c. These measurements were interpreted on the basis of Eq. (18); σ (as contrasted with the resistivity) falls smoothly with $P - P_\mathrm{c}$ according to a power law whose exponent is $\mu \equiv d\nu = 1.1$. In Fig. 10 there is shown the change in σ with temperature at pressures barely exceeding the critical value P_c. One sees that the anticipated power law is accurately obeyed with $\sigma \sim T^{0.22}$, whence $d/z = 0.22$.

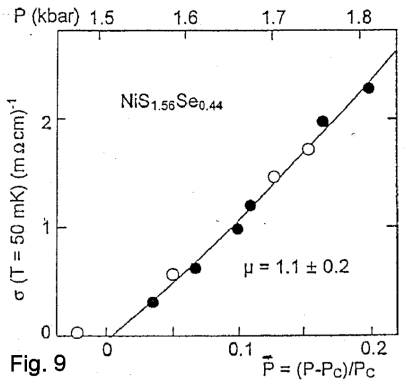

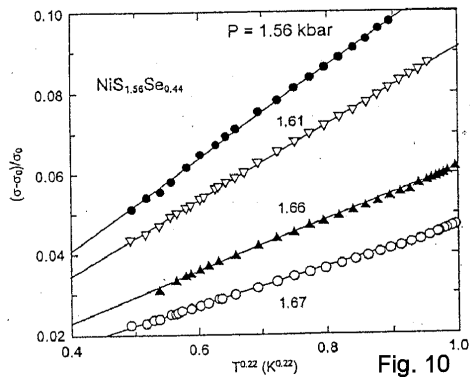

Fig. 9. Electrical conductivity σ at 50 mK of a single crystal of $NiS_{1.56}Se_{0.44}$ as a function of pressure above the critical pressure $P_\mathrm{c} = 1.51$ kbar.

Fig. 10. Electrical conductivity σ as a function of temperature of a single crystal of $NiS_{1.56}Se_{0.44}$ at pressures barely exceeding the critical pressure P_c. Let us note the power law dependence $\sigma \sim T^{0.22}$.

A critical test for the applicability of this analysis is the requirement that with $p \equiv (P - P_\mathrm{c})/P_\mathrm{c}$ materials close to criticality should obey the relation $\sigma(p, T) = p^{\nu d} f[(T/p^{\nu z})^{d/z}, 1]$ where f is a universal function of the indicated variables. This reflects the fact that near criticality all length scales greatly exceed those of atomic distances. It follows from the above that

$$\sigma/p^{\mu} \sim T^{d/z}/p^{d\nu} = (T/p^{z\nu})^{d/z}, \tag{20}$$

when plotted as ln (σ/p^{μ}) vs. ln $(T/p^{z\nu})$, should produce a single curve onto which all data points collapse. The extent to which this is the case is shown in Fig. 11, thus conforming to a stringent test for the applicability of the above concepts.

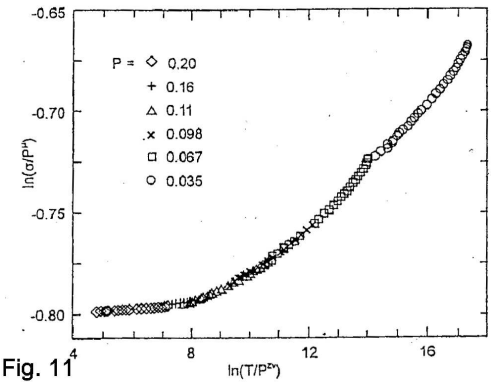

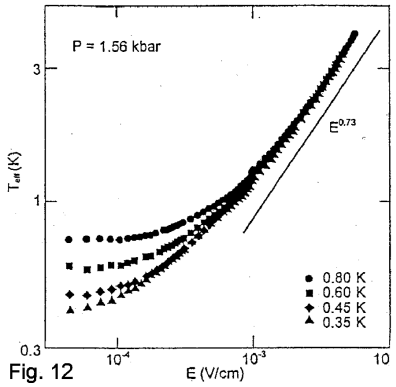

Fig. 11. Reduced data plots showing the collapse of the various electrical conductivity measurements onto a single curve, as a test of the applicability of the various scaling laws cited in the text.

Fig. 12. Nonohmic electrical conductivity measurements on $NiS_{1.56}Se_{0.44}$ at 350–800 mK at a pressure $P = 1.56$ kbar as a function of the applied electric field $\mathcal{E}$. Let us note the merging of the data points at high electric fields. The slope of the linear part of the curve is a measure of the critical exponent z.

The three exponents introduced earlier may be determined individually by an additional set of nonlinear electrical conductivity measurements in high applied electric fields $\mathcal{E}$. Here the relevant length scale is the mean free path $l_{\mathcal{E}}$ near the critical point, with a corresponding time scale $\xi_{\tau} \sim \xi^z \sim l_{\mathcal{E}}^z$. The energy gain by an electron in the accelerating field is $E = e\mathcal{E}l_{\mathcal{E}}$ while the energy fluctuations due to the uncertainty principle read $\hbar/\xi_{\tau} \sim l_{\mathcal{E}}^{-z}$. On equating these two relations we obtain $l_{\mathcal{E}} \sim \mathcal{E}^{-1/(z+1)}$. The authors defined a corresponding temperature by $k_{\mathrm{B}}T_{\mathrm{eff}} = e\mathcal{E}l_{\mathcal{E}}$, where the conversion from σ to T_{eff} also involved the electrical measurements in the ohmic region. In the nonohmic range the conductivity is governed by the magnitude of $\mathcal{E}$. For sufficiently high values all measurements should merge onto a single curve with $T_{\mathrm{eff}} \sim \mathcal{E}^{z/(z+1)}$. This expectation is met, as is evident from inspection of Fig. 12 for a set of temperatures in the range 0.35 to 0.80 K. The slope of the merged curves leads to a value $z = 2.7$.

As a result of these experiments one encounters the following values for the critical exponents:

$\nu = 1.7$, the correlation length in the relation $\xi(K) \sim |\delta|^{-\nu}$,

$z = 2.7$, the dynamical scaling exponent in the relation $\xi_t(K) \sim \xi^z$,

$d = 0.59$, the scaling exponent in the relation $O(k, \omega, K) = \xi^d O(k\xi, \omega\xi_t)$.

The experiments have shown that under the specified conditions the electron assembly in $NiS_{1.56}Se_{0.44}$ does undergo a quantum phase transition at extremely low temperatures. However, the above values that characterize the transition differ from those normally associated with quantum critical phenomena. Usually the dimension d is found to be close to an integer; the above remaining exponents also fall outside normally accepted range. This might be an indication that close to 0 K the electron assembly constitutes a new universality class, though this speculation requires confirmation. In any case, the experiments illustrate the interesting quantum mechanical phenomena that are observable in systems where electron correlations predominate.

9. Concluding remarks

In surveying the above information it is clear that the V_2O_3 and NiS_2 systems are poised at the borderline between itinerant and localized electron configurations. This renders possible a study of events where these systems are forced to undergo transformations from one state to the other. The underlying theoretical interpretation requires the use of models that go beyond the elementary electron gas approximations. The basic ideas outlined above are very simple and lead to a semiquantitative understanding of the observations. However, a full exploration of all consequences [19] becomes rather complicated, and has therefore not been taken up here. Lastly, under appropriate conditions the electron assemblies in these systems can be made to exhibit critical phenomena, both of the classical type for fluids and of effects driven by quantum fluctuations.

Acknowledgments

The author wishes to thank Mr. Ross Hoehn in the Department of Chemistry, for performing the calculation involved in generating Fig. 4. The author is obviously enormously indebted to all the individuals who carried out the difficult preparation of samples and the meticulous experimental studies. Most of all, he is grateful for the many years of collaboration with Professor Spałek, who provided the penetrating theoretical insights for interpreting the experimental work at Purdue University, and who thereby taught the author the basics of electron correlation phenomena.

References

[1] J.M. Honig, L.L. Van Zandt, *Ann. Rev. Mater. Sci.* **5**, 225 (1975); N.F. Mott, in: *Festkoerperprobleme*, Vol. 19, Ed. J. Treusch, Vieweg, Braunschweig 1979, p. 341; J.M. Honig, *J. Solid State Chem.* **45**, 1 (1982); J.M. Honig, J. Spałek, *Proc. Indian Natl. Sci. Acad. A* **52**, 232 (1986); N.F. Mott, *Metal–Insulator Transitions*, 2nd ed., Taylor & Francis, London 1990; M. Yethiraj, *J. Solid State Chem.* **88**, 53 (1990); M. Yethiraj, J.M. Honig, in: *Advances in Synthesis and Reactivity of Solids*, Vol. 2, Ed. T.E. Mallouk, JAI Press, London 1994, p. 235; J.M. Honig, J. Spałek, *Chem. Mater.* **10**, 2910 (1998); J.M. Honig, J. Spałek, *Current Opinion Solid State Mater. Sci.* **5**, 269 (2001); J.M. Honig, *Recent Res. Devel. Chem. Physics* **5**, 511 (2004).

[2] M. Foëx, *Compt. Rend. Acad. Sci. (Paris)* **223**, 1126 (1946); **229**, 880 (1949).

[3] D.B. McWhan, T.M. Rice, J.P. Remeika, *Phys. Rev. Lett.* **23**, 1384 (1969); A. Menth, J.P. Remeika, *Phys. Rev. B* **2**, 3756 (1970); D.B. McWhan, J.P. Remeika, *Phys. Rev. B* **2**, 3734 (1970); D.B. McWhan, J.P. Remeika, *Phys. Rev. Lett.* **27**, 941 (1971); D.B. McWhan, A. Menth, J.P. Remeika, W.F. Brinkman, T.M. Rice, *Phys. Rev. B* **7**, 1920 (1973).

[4] H. Kuwamoto, J.M. Honig, J. Appel, *Phys. Rev. B* **22**, 2626 (1980).

[5] S.A. Shivashankar, J.M. Honig, *Phys. Rev. B* **28**, 5695 (1983).

[6] T.A. Bither, R.J. Bouchard, W.H. Cloud, P.C. Donahue, W.J. Siemons, *Inorg. Chem.* **7**, 2208 (1968); R.J. Bouchard, J.L. Gillson, H.S. Jarrett, *Mater. Res. Bull.* **8**, 489 (1973); H.S. Jarrett, R.J. Bouchard, J.L. Gillson, G.A. Jones, S.M. Marcus, J.F. Weiher, *Mater. Res. Bull.* **8**, 877 (1973).

[7] X. Yao, J.M. Honig, *Mater. Res. Bull.* **29**, 709 (1994); X. Yao, J.M. Honig, T. Hogan, C. Kannewurf, J. Spałek, *Phys. Rev. B* **54**, 17469 (1996); X. Yao, S. Ehrlich, G. Liedl, T. Hogan, C. Kannewurf, J.M. Honig, *Mater. Res. Soc. Proc.* **453**, 291 (1997); X. Yao, Y.-K. Kuo, D.K. Powell, J.W. Brill, J.M. Honig, *Phys. Rev. B* **56**, 7129 (1997); J.M. Honig, *Mater. Res. Soc. Proc.* **547**, 425 (1999).

[8] D.D. Sarma, S.R. Krishnakumar, E. Weschke, C. Schüssler-Langeheine, C. Mazumdar, L. Kilian, G. Kaindl, K. Mayima, S.-I. Fujimori, A. Fujimori, T. Miyadai, *Phys. Rev. B* **67**, 155112 (2003); S.R. Krishnakumar, D.D. Sarma, *Phys. Rev. B* **68**, 155110 (2003).

[9] M.C. Gutzwiller, *Phys. Rev. Lett.* **10**, 159 (1963); *Phys. Rev.* **137**, A1726 (1965).

[10] W.F. Brinkman, T.M. Rice, *Phys. Rev. B* **2**, 4302 (1971); in: *Critical Phenomena Alloys, Magnets and Superconductors*, Eds. R.E. Mills, E. Ascher, R. Jaffe, McGraw-Hill, New York 1971, p. 593.

[11] J. Spałek, A.M. Oleś, J.M. Honig, *Phys. Rev. B* **28**, 6802 (1983); J. Spałek, A. Datta, J.M. Honig, *Phys. Rev. Lett.* **59**, 728 (1987); J. Spałek, M. Kokowski, J.M. Honig, *Phys. Rev. B* **39**, 4175 (1989).

[12] J. Spałek, P. Gopalan, *Phys. Rev. Lett.* **64**, 2823 (1990).

[13] J.M. Honig, *Recent Res. Devel. Chem. Phys.* **5**, 511 (2004).

[14] S.A. Carter, T.F. Rosenbaum, P. Metcalf, J.M. Honig, *Phys. Rev. B* **48**, 16841 (1993).

[15] X. Yao, Y.-K. Kuo, D.K. Powell, J.W. Brill, J.M. Honig, *Phys. Rev. B* **56**, 7129 (1997).

[16] P. Limelette, A. Georges, D. Jérome, P. Wzietek, P. Metcalf, J.M. Honig, *Science* **302**, 89 (2003).

[17] A. Husmann, D.S. Jin, Y.V. Zastavker, T.F. Rosenbaum, X. Yao, J.M. Honig, *Science* **274**, 1874 (1996); A. Husmann, J. Brooke, T.F. Rosenbaum, X. Yao, J.M. Honig, *Phys. Rev. Lett.* **84**, 2465 (2000).

[18] S.L. Sondhi, S.M. Girvin, J.P. Carini, D. Shahar, *Rev. Mod. Phys.* **69**, 315 (1997).

[19] J. Spałek, M. Kokowski, J.M. Honig, *Phys. Rev. B* **39**, 4176 (1989).